4 High resolution modelling

4.1 Introduction

Storm 3 and 4 were the most important storms recorded at the instrumental transect from the point of view of H_s magnitude. As said previously, the first one was a characteristic northwest fetch-limited growth event; the second one was a characteristic eastern fully-developed wave storm. Neither of them was satisfactorily predicted by the operational model. From the point of view of previous wave modelling, limitations were specifically reported for fetch-limited growth events, which are still not fully understood. Indeed, Cavaleri and Bertotti (2004) described smaller model errors at longer fetch and reported a reduction of the errors with higher resolution models. More specifically, Bolaños (2004) pointed out that predictions during fetch-limited conditions in the region of study are subject to the spatial resolution of the models. Also, storm 3 was the only fetch-limited and mainly unimodal event recorded along the instrumental transect. For all these reasons, the objective of this chapter was to increase the resolution of a wave model, using higher resolution wind fields, to model storm 3: a particular fetch-limited growth event.

During the selected storm event, a high pressure system was located over the Azores, and a deep low pressure system was placed over the UK. They were both imposing west and northwest winds over Catalonia, as they moved across Europe towards the East. H_s time series reported three peaks of different magnitude at the most offshore station A-dw(D), where H_s reached a maximum 3.5m for a 55km long fetch. The energy spectra were fairly unimodal, which means that although the storm was considered to be unimodal, seldom a secondary opposing wave train was detected. However, no open-sea boundary conditions were used, for the swell wave train was not energetic enough to be relevant. The energy content of the swell component was assessed from the measurements at D-sw(S): the most coastal location. Because of its location close to the coast, the sea peak was not energetic enough to override the swell peak and thus, the energy content of the latest could be assessed using visual analysis. During the first peak of the storm (10th of December 2007) the swell energy peak was approximately 0.1 m^2/Hz (Figure 2-12). At approximately the same time, the sea peak at A-dw(D) reached 14 m^2/Hz, at E-iw(D) it was 6 m^2/Hz, and at B-iw(S) it was 3 m^2/Hz (Figure 2-10 – left panel). The swell peak did not account for more than 3% of the total energy, and therefore, the non-inclusion in the simulations was not expected to significantly influence the simulations.

This event was particularly challenging in terms of wave modelling because of its short fetch, but also in terms of wind modelling, because their performance in such complex coastal areas was not yet fully assessed.

4.1.1 MM5 atmospheric model

The SMC, member of the RIMA project, obtained the wind fields using the atmospheric model MM5 vs.3.5, which is a nonhydrostatic primitive-equation model that uses terrain following coordinates (Grell et al. 1994). The initial and boundary conditions were provided by the European Centre for Medium range Weather Forecast (ECMWF) analysis data at 0.5° spatial resolution every 24h. Three simulations were run with horizontal resolutions of approximately 36, 12 and 4km. The mother domain covered southwest Europe; the second domain covered Catalonia and south France, and the finer domain (4km) covered only Catalonia (northeast Spain) (Figure 4-1). The temporal resolution of the finer grid was 3h. Each simulation of the model assimilated observational data from surface (METAR, SAO, SHIP) and upper air sounding data (RAOB data). For the microphysical processes Schultz (1995) explicit scheme and Grell (1993) convective parameterization were used. The planetary boundary layer was modelled using the MRF scheme, and the radiation scheme used the Rapid Radiative Transfer Model (RRTM). The configuration of the different nested simulations of the MM5 model is summarized in Table 4-1.

Table 4-1. Configuration of the different nested simulations of the MM5 model: Number of grid points in the X, Y and Z coordinates, Initial conditions (IC) and Lateral Boundary Conditions (LBC), and resolution in km.

Domains	X. Y. Z (grid points)	IC/LBC	Resolution (km)
MM5.36km	104x96x36	ECMWF/GFS	36
MM5.12km	70x70x30	MM5-36km	12
MM5.4km	80x80x30	MM5-12km	4

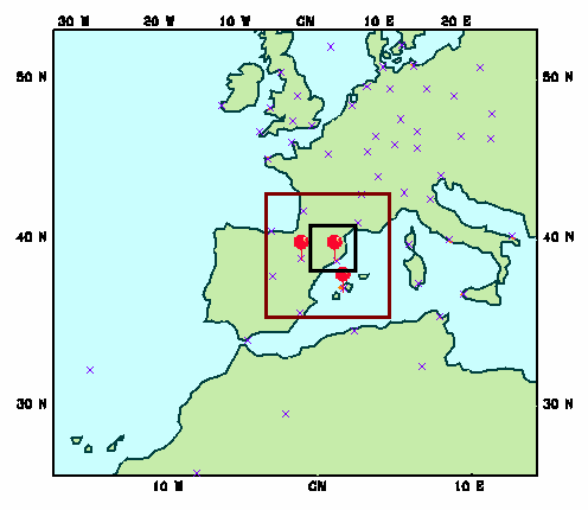

Figure 4-1. MM5 atmospheric model 36, 12 and 4km horizontal resolution domains (the latter within the black square). The assimilated observational data is depicted in red and violet.

4.1.2 SWAN wave model

The SWAN (Simulating Waves Nearshore) wave model is a third generation model that was specifically designed to better resolve the physics in shallow waters. It is based on the action balance equation (Equation 3-2) for given source and sink functions, without any previous assumption of the spectral shape (Ris 1997). SWAN uses an implicit scheme for wave propagation, which is computationally more economic in shallow waters than the other state-of-the-art third generation models (including WAM), and provides additional robustness to the model. SWAN deep water physics are taken from WAM model, as described in Komen et al. (1994), but it also includes additional source terms especially relevant in shallow waters, such as the depth-induced breaking and triad wave-wave interactions (Ris 1994; Monbaliu et al. 2004).

The action balance equation solved by SWAN in the frequency and directional space is:

$$\frac{\partial}{\partial t}N(\sigma,\theta)+\frac{\partial}{\partial x}c_x N(\sigma,\theta)+\frac{\partial}{\partial y}c_y N(\sigma,\theta)+\frac{\partial}{\partial \sigma}c_\sigma N(\sigma,\theta)+\frac{\partial}{\partial \theta}c_\theta N(\sigma,\theta)=\frac{S(\sigma,\theta)}{\sigma}$$

Equation 4-1

On the right-hand side of this equation, $S(\sigma,\theta)$ is the energy source term. It is usually represented as the sum of generation (S_{in}), dissipation (S_{ds}) and non-linear interaction (S_{nl}) processes (Equation 3-5). Each one of these separate source terms represents different physical processes. S_{in} represents

the wave energy input from the wind; S_{ds} the energy dissipation due to whitecapping, bottom interaction, and deep-induced breaking in shallow waters; and S_{nl} the wave-wave interactions through quadruplet and triad interactions. In the literature there exist many different parameterizations that attempt to describe these processes. In SWAN they can be selected according to particular requirements; they are described in next chapter.

SWAN was previously implemented in the study region by Bolaños et al. (2007). They implemented two wave models in the region (WAM and SWAN) and compared their performance. Although the differences were not significant, SWAN seemed to predict slightly better the magnitude of the integrated parameters at the storm peak. In contrast, the spectral shape was less accurate than using WAM. Nonetheless, SWAN is a very user-friendly wave model and it has a quite extended user's community. For these reasons, SWAN was chosen to assess the impact of an increase of resolution on the wave predictions in the region.

In this work the SWAN 40.72AB version was used and will be referred to as SWAN. It was initially forced using the wind input at 10m height from the MM5 finer simulation (0.04° spatial resolution and 3h temporal resolution). The SWAN wave model was run using a 0.01° (approx. 1km) spatial resolution and an output temporal resolution of 1h. The first time step (wind input from the 7th December 2007 at 00h) was run in stationary mode to reach convergence. After it, the predictions were obtained in non-stationary mode. The directional resolution was set to 10°, and the frequency resolution were 40 frequencies distributed logarithmically ($\Delta f / f = 0.119$) between 0.01-1Hz. The computational time step was set to 20 min. For the basic configuration SWAN was used with the default wind growth source functions, quadruplet interactions and whitecapping sink functions, which are due to Komen et al. (1984) (hereafter KOM). The numerical method used was the BSBT scheme. The bottom friction was not activated and neither were the triads. The model domain is depicted in Figure 4-2.

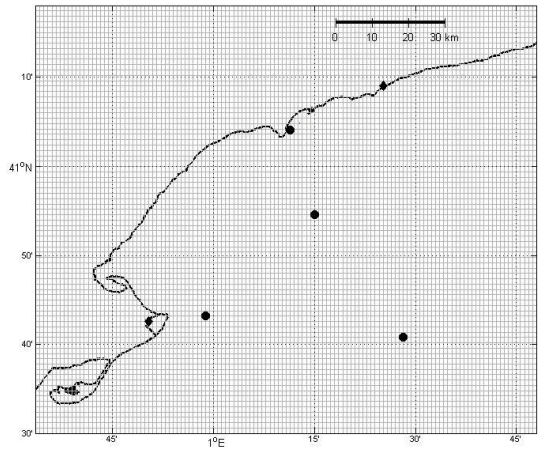

Figure 4-2. SWAN model domain and grid resolution. The black dots are the instruments described in Chapter 2.

4.2 Methodology

The performance assessment of the basic configuration of the high-resolution SWAN model was conducted using the same analysis described in Chapter 3: a visual comparison and a statistical analysis.

The qualitative analysis consisted of a visual comparison of the wind and wave data registered during storm 3 (and described in Chapter 2), in terms of WS, WiD (wind model) and H_s, T_p and PWD (wave model). Also, the wave model output included the prediction of the energy and directional spectra at the location of the different instruments. Therefore, the predicting skills of the operational model in terms of the energy spectra were also assessed. The accuracy in predicting the directional spectra will be addressed in future work.

The statistical analysis is also performed using the same statistical estimators described in Chapter 3: bias, RMSE, MAE, RMAE, and SI, percentage of error and scatter plots.

4.3 Results

The validation of the WS from the atmospheric model was done by means of the coastal meteorological stations and the offshore buoy. The results show that WS was generally over-predicted, especially at the coastal stations, EMA-T and EMA-U, where the WS over-prediction reaches 3.5-4 m/s bias (100% error). More accurate predictions were obtained at the offshore buoy A-dw(D) (Figure 4-3), where the bias was, nonetheless, 2m/s (25% over-prediction).

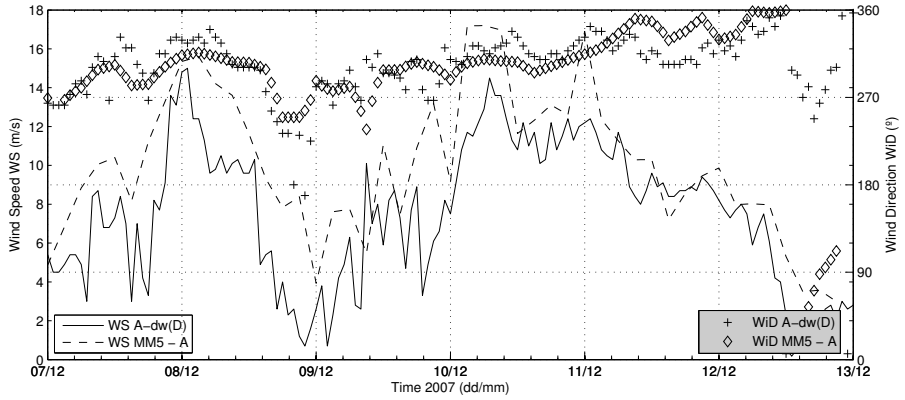

Figure 4-3. MM5 wind speed (WS) and wind direction (WDir) validation: predictions (dashed lines, ◊) and observations (solid lines, +) at the offshore buoy A-dw(D).

Even though MM5 WS were over-predicted, H_s from the high resolution SWAN model was still under-predicted. However, higher resolution SWAN predicted better the peaks of the storm and its magnitude than the operational coarser resolution model: H_s under-prediction at the peak of the storm improved on the order of 1m (Figure 4-4). As described in Chapter 3, the operational model reported up to 1.5m (-50%) of under-prediction. With the finer mesh the under-prediction at the peak of the storm at the most offshore station was 0.5m (-17%) (Figure 4-5). Also, proper magnitude wave parameters at coastal locations (1km offshore) were obtained (Figure 4-6). Additionally, higher resolution SWAN model was able to properly resolve the temporal occurrence of the storm peaks and to reproduce some of the differences in H_s and PWD observed at the different buoys.

Indeed, the H_s peak reported at B-iw(S) but not at E-iw(D) the 9th December 07 at midday was predicted by the simulations, although slightly shifted in time. Also, the deviation of PWD between E-iw(D) and A-dw(D) was reproduced. It must be noted that eastern PWD recorded the 9th around midnight were not properly reproduced because they correspond to the underlying eastern swell, which was not considered in these simulations. When the NW wind decreased, its associated sea peak decreased faster, and the most energetic peak was, for a few hours, the eastern swell component. However, and as discussed in the introduction of this chapter, not considering the swell component could not be the reason for the observed under-prediction because its magnitude was much smaller than the reported under-prediction.

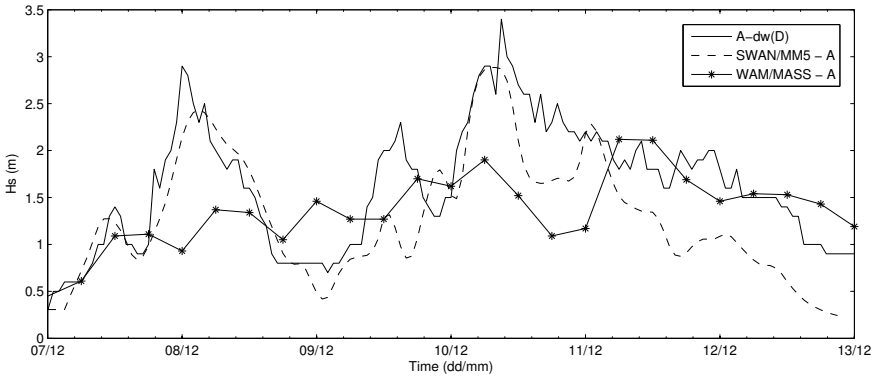

Figure 4-4. Measured and predicted H_s at A-dw(D). The solid line depicts the observations at the buoy. The pointed line is the prediction issued with the coarse resolution (18km) operational WAM model; the dashed line is the prediction obtained using higher resolution (1km) SWAN model.

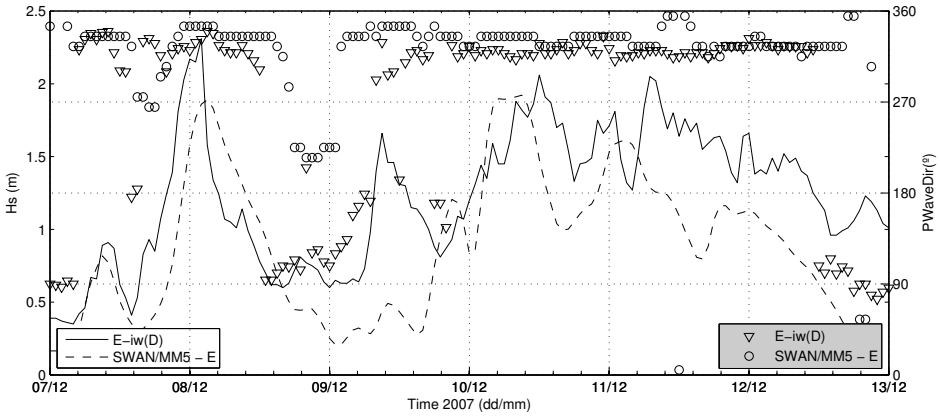

Figure 4-5. Measured and predicted H_s (left y-axis) and PWD (right y-axis) at E-iw(D). The solid line and the triangles depict the observations at the buoy. The dashed line and the circles are the predictions issued with high resolution SWAN model.

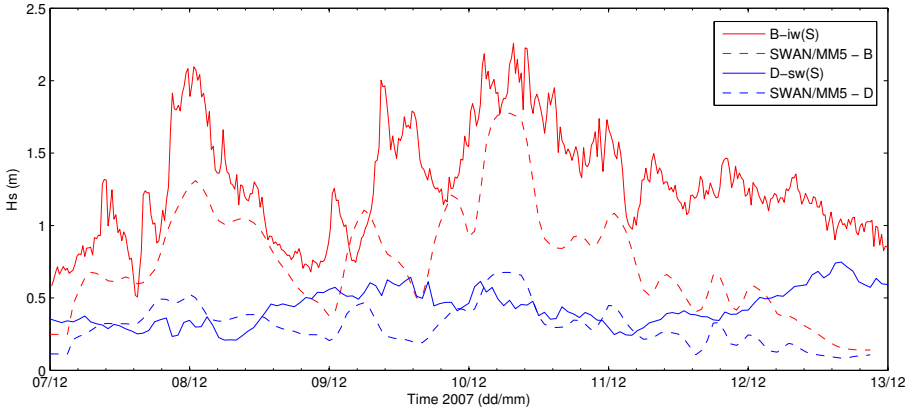

Figure 4-6. Measured and predicted H_s at B-iw(S) and D-sw(S). The solid lines depict the observations at the buoy. The dashed lines are the predictions issued with high resolution SWAN model.

Although the improvement was evident, the hindcasted H_s fields were still under-predicted (at some points up to 1m (-30%)) (Figure 4-6, Figure 4-5) and the reason could not be directly associated to under-predicted WS.

Inaccuracies were also observed in the model's prediction of the spectral shape (Figure 4-7). The energy at the peak of the spectrum was generally under-predicted, in agreement with H_s under-predictions, and the peak frequency was over-predicted (T_p under-predicted). The differences decrease with fetch: as the fetch increases, the peak frequency moves to lower frequencies and the energy peak increases, reducing the differences with the observations. The observed improvement with fetch was already described by Cavaleri and Bertotti (2004). The general under-prediction of T_p was already reported for SWAN by other authors (e.g. Siddons et al. 2009). Nonetheless, it is interesting because it was a systematic under-prediction and because the operational model predictions of T_p depended on T_p's magnitude (over-prediction above 7.5s).

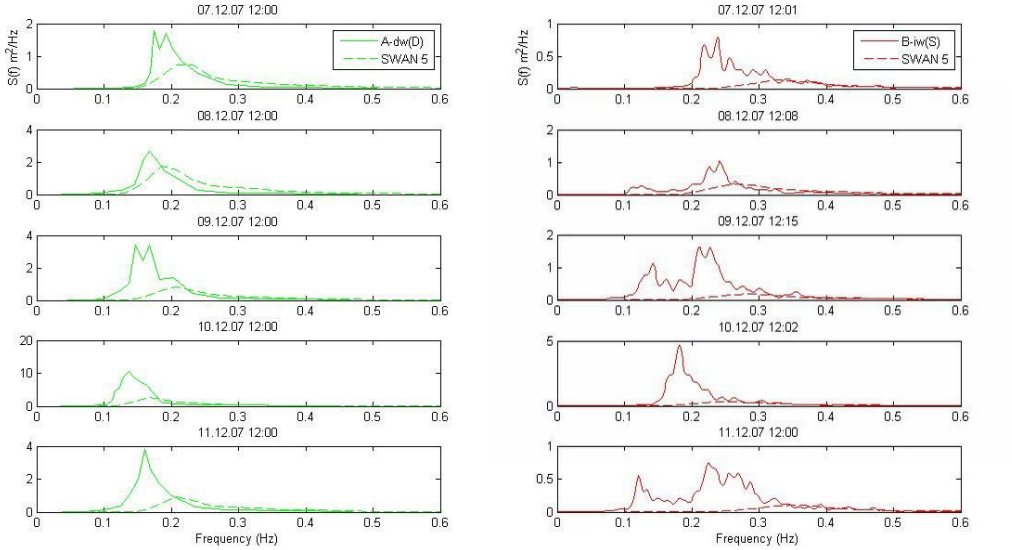

Figure 4-7. Measured and predicted energy spectra at A-dw(D) (left; fetch: 55km) and B-iw(S) (right; fetch: 20km). Solid lines represent observed data and dashed lines represent SWAN predictions. Each plot corresponds to the energy spectra at 12h every day during storm 3.

The results obtained from the statistical analysis (Figure 4-8) do not reproduce the significant improvement observed from the visual analysis, which was associated with the resolution increase (except at the most coastal location). In fact, when comparing the different statistical parameters considered in the analysis, the error estimators of the coarser resolution model are lower than the estimators of the higher-resolution model. These results support what was reported by different authors and stated again in Chapter 3: statistical estimators must be handled carefully because they may induce to misleading conclusions.

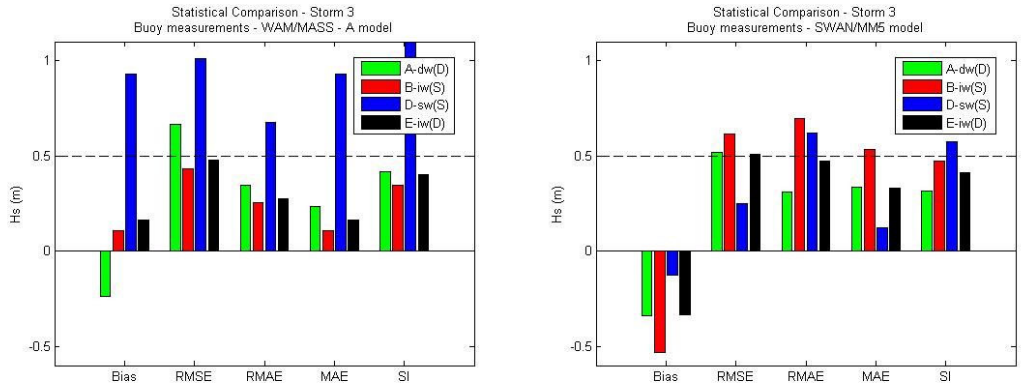

Figure 4-8. Statistical analysis in terms of H_s and bias, RMSE, RMAE, MAE and SI at the different measuring instruments (A-dw(D), B-iw(S), C-sw(D), D-sw(S) and E-iw(D)) during storm 3; using coarse resolution WAM model (left) and higher resolution SWAN model (right).

However, H_s corresponding scatter plots do verify the improvement obtained with higher resolution models (Figure 4-9). T_p's scatter plot is not shown here because the agreement is not conclusive because the high-period swell measurements were not simulated.

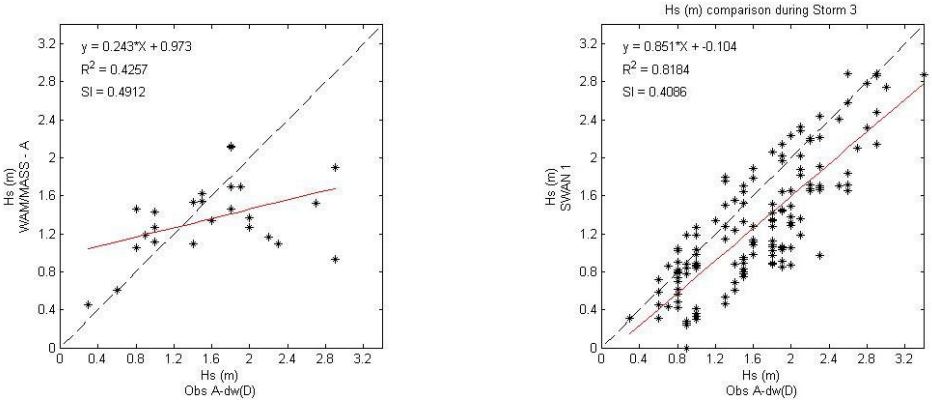

Figure 4-9. H_s scatter plot. Observations at A-dw(D) and simulations from WAM (left plot) and SWAN (right plot) during storm 3. The red line is the linear equation that best fits the data points (upper-left corner of the plot). The dashed line indicates the ideal fit (1:1 linear equation).

4.4 Discussion

According to the results presented above, it is accurate to affirm that an increase of the wind and wave models significantly improved H_s predictions (13% of improvement), even though the statistical results were not conclusive. Indeed, the statistical estimators were confirmed to be strongly inaccurate to assess the performance of the wave model. These results reinforce the importance of visual assessments of the time series. Scatter plots also provide a useful additional tool for the comparison.

Compared to the operational wave model, the higher resolution model produced reasonable predictions near the coast, and also reproduced the spatial differences between instruments described in Chapter 2. Thus, it is confirmed that higher resolution wind fields make possible to reproduce the spatial differences that were not predicted otherwise. Nonetheless, the systematic under-prediction described in the literature (Cavaleri and Bertotti 2004; Bolaños et al. 2004), although reduced, was still observed. The reason could not be directly attributed to the wind input because the wind fields seemed to be rather over-estimated.

Because the input wind field is the most important factor forcing wave predictions, it is necessary to check what wind fields are the best winds available to simulate wave storms in the study region. The cause of the under-prediction should first be searched for in the wind input, and will be addressed in next chapter.

Also, the performance of the model in other wave conditions (fully-developed growth and bimodal storms) must be also studied to fully assess the improvement provided when using high resolution models.